

Chaotic variability of the magnetic field at Earth’s surface driven by ionospheric and space plasmas

Alexander Bershadskii

ICAR, P.O. Box 31155, Jerusalem, 91000, Israel

E-mail: bershads@gmail.com

Abstract

It is shown that the universal chaotic/turbulent processes in space (solar wind and magnetosphere) and in ionospheric plasmas drive the chaotic temporal variability and determine the level of randomness of the magnetic field at Earth’s surface in the temporal range from a few hours to a few years. The results of observations provided by the spacecraft and satellite missions, and the global magnetic observatory network were used for this purpose. A good agreement has been established between the results of observations and a theoretical approach based on the Kolmogorov-Iroshnikov phenomenology in the frames of distributed chaos notion.

1. Introduction

There are two main sources of the temporal variability of the magnetic field at Earth’s surface. The inner source is related to magnetic field generation by the motion of the liquefied and charged iron in the outer core of the Earth and has comparatively long-term dynamics (see for recent reviews [Constable and Constable, 2023](#); [Bershadskii, 2024a](#) and references therein). Another (external) main source is related to the complex interaction of the near-Earth solar wind with the coupled magnetosphere-polar ionosphere structure ([Borovsky, 2020](#); [Telloni et al., 2020](#)). The external source of the magnetic field variability at Earth’s surface is stronger than the internal source at periods lesser than the 11-year solar cycle (see, for instance, paper of [Constable and Constable 2023](#) and references therein). An additional important external source of the temporal variability of the magnetic field is related to thermal electric currents in the ionosphere on the heated day side of the globe, which results in the appearance of a prominent daily spectral peak (and its harmonic) in the magnetic energy spectrum. The seasonal variations of the ionosphere heating also result in the spectral peaks corresponding to the 1 year and 6 months ([Constable and Constable, 2023](#)). One can see that all these external sources of variability are related to the Sun.

The considerable range from a few hours to a few years, where the space source dominates over the inner source of the temporal variability of the magnetic field at Earth’s surface, will be the subject of the present investigation. This range of scales can provide valuable information on the physical processes in the highly chaotic dynamics of the solar

wind, magnetosphere, and ionosphere and their interaction.

In Section 2 of the paper a fundamental magnetohydrodynamic invariant - magnetic helicity, which will play a crucial role in the paper's consideration, has been introduced. Section 3 describes the magneto-inertial range of scales driven by magnetic helicity. Section 4 describes the spectral properties of smooth chaotic dynamics and randomization of the magnetic field in terms of distributed chaos. Section 5 shows the applicability of this theoretical notion to the solar wind (just before it impacts the Earth's magnetosphere) and magnetosphere-ionosphere magnetized plasmas using the data obtained during different spacecraft and satellite missions. Section 6 reports the conformity of the spectral properties of the chaotic (random) magnetic field at Earth's surface to those observed in the space plasmas in a wide range of frequency scales and even for the geomagnetic storm time. In Section 7 we discuss the implications of the obtained results for space weather forecasting and their limitations.

The consideration is heavily based on the observations obtained by probes onboard different spacecraft and satellite missions such as the Solar Dynamics Observatory spacecraft (Helioseismic and Magnetic Imager), the Wind spacecraft (which was put in a Lissajous orbit around the Lagrange point L1 to investigate the undisturbed solar wind just before it impacts the Earth's magnetosphere), the Cluster multispacecraft (downstream of the quasiparallel bow shock), Swarm A satellite (vector field magnetometer for the ionospheric magnetic field measurements). Also, the spectral data obtained by the real-time global magnetic observatory network (the ground-based special magnetometers recording the absolute level of the time-varying magnetic field at the Earth's surface) as well as by a special station in South Australia were used for the analysis of the variability of the magnetic field at Earth's surface in regular and geomagnetic storm time.

2. Magnetic helicity

In ideal magnetohydrodynamics we have three fundamental quadratic invariants: total energy, magnetic and cross helicity (see, for instance, [Moffatt and Tsinober, 1992](#) and references therein).

The average magnetic helicity density is

$$h_m = \langle \mathbf{A} \cdot \mathbf{B} \rangle \quad (1)$$

where the magnetic field is $\mathbf{B} = [\nabla \times \mathbf{A}]$ (\mathbf{A} is the vector potential), $\nabla \cdot \mathbf{A} = 0$ and $\langle \dots \rangle$ denotes a spatial average.

When a uniform mean magnetic field \mathbf{B}_0 is present the magnetic helicity is not an invariant. A modified magnetic helicity density was introduced for this case in the paper ([Matthaeus and Goldstein, 1982](#))

$$\hat{h}_m = h_m + 2\mathbf{B}_0 \cdot \langle \mathbf{A} \rangle \quad (2)$$

where $\mathbf{B} = \mathbf{B}_0 + \mathbf{b}$, $\mathbf{A} = \mathbf{A}_0 + \mathbf{a}$, and $\mathbf{b} = [\nabla \times \mathbf{a}]$. It is shown by [Matthaeus and Goldstein \(1982\)](#) that at certain restrictions on the boundary conditions

$$\frac{d\hat{h}_m}{dt} = 0, \quad (3)$$

i.e. the modified magnetic helicity is still an ideal invariant in the magnetohydrodynamics (see also [Shebalin, 2013](#)).

3. Magneto-inertial range of scales

For the high Reynolds numbers an inertial range of scales, determined by the kinetic energy dissipation rate ε only, is considered in hydrodynamic turbulence. According to the Kolmogorov phenomenology energy is freely (with negligible dissipation) transferred through this range to the sufficiently small scales where it is dissipated due to viscosity ([Kolmogorov, 1941](#)) (see also [Monin & Yaglom, 2007](#) and references therein). In magnetohydrodynamics (and even at the kinetic scales) a magneto-inertial range of scales was recently introduced ([Bershadskii, 2024b](#)). In this range, two parameters: the magnetic helicity dissipation rate ε_{h_m} and the total energy dissipation rate ε determine the magnetic field dynamics.

In the case of a nonzero (considerable) mean magnetic field the energy dissipation rate ε should be replaced by a more appropriate parameter ($\varepsilon\tilde{B}_0$) ([Iroshnikov, 1963](#)). Here $\tilde{B}_0 = B_0/\sqrt{\mu_0\rho}$ is the normalized mean magnetic field, which has the same dimension as velocity (the Alfvén units). In the original Iroshnikov's phenomenology ([Iroshnikov, 1963](#)) the eddies, which were considered by Kolmogorov for hydrodynamic, were replaced by the Alfvén wave-packets propagating in opposite directions along the mean magnetic field. The applicability of the Kolmogorov-like and Iroshnikov-like phenomenologies to magnetohydrodynamics was vigorously discussed for decades and different modifications were suggested but the main idea: to use ε or ($\varepsilon\tilde{B}_0$) as the only important dimensional parameter in the inertial range of scales, was remained.

For the magneto-inertial range in the presence of a considerable mean magnetic field the dimensional considerations result in ([Bershadskii, 2024b](#))

$$B_c \propto \varepsilon_{h_m}^{1/2} (\varepsilon\tilde{B}_0)^{-1/8} k_c^{1/8} \quad (4)$$

and

$$B_c \propto \varepsilon_{h_m}^{1/2} (\varepsilon\tilde{B}_0)^{-1/6} f_c^{1/6} \quad (5)$$

where B_c is the characteristic value of the magnetic field, k_c and f_c are the characteristic wavenumber and frequency respectively, ε_{h_m} is the modified magnetic helicity dissipation rate. Following the Kolmogorov-Iroshnikov phenomenology within the magneto-inertial range not only the energy but also the magnetic helicity transfer is carried out practically without dissipation.

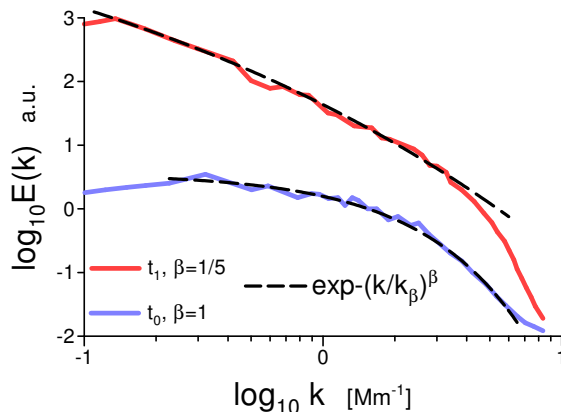


Figure 1: Magnetic energy spectra calculated for the emerging solar active region NOAA 12219: t_0 is the moment of the emergence onset (bottom curve) and t_1 is the moment of the maximal magnetic flux (top curve). The data were obtained by the Solar Dynamics Observatory spacecraft.

4. Smooth chaotic dynamics and randomization of magnetic field

The spectral analyses based on the notion of smoothness can be useful for the quantitative classification of chaotic/turbulent regimes according to their randomness. For the smooth chaotic magnetohydrodynamics the stretched exponential spectra are typical (Bershadskii, 2024b)

$$E(k) \propto \exp -(k/k_\beta)^\beta, \quad E(f) \propto \exp -(f/f_\beta)^\beta \quad (6)$$

here $1 \geq \beta > 0$, k is the wavenumber, and f is the frequency. For deterministic chaos $\beta = 1$

$$E(k) \propto \exp -(k/k_c), \quad E(f) \propto \exp(-f/f_c) \quad (7)$$

is typical (see, for instance, Frisch and Morf, 1981; Brandstater and Swinney, 1987; Maggs and Morales, 2011, 2012a,b; Khurshid et al., 2018).

For $1 > \beta$ the dynamics is smooth but not deterministic (Wu et al., 1990). This type of dynamics will be called distributed chaos (a clarification of the term will be given below). Another term for this type of dynamics: soft turbulence, was suggested by Wu et al. (1990). The non-smooth dynamics (hard turbulence Wu et al., 1990) is characterized by the scaling (power-law) spectra. The value of the β can be used as a measure of randomization in this approach: the further the value of the parameter β is from the deterministic value $\beta = 1$ (i.e. smaller the β) the randomization is stronger. For $\beta \rightarrow 0$ we have the hard turbulence with its power-law spectra

Figure 1, for instance, shows the magnetic energy spectra at the onset (t_0) of the emergence of solar active region NOAA 12219 (the bottom curve) and at the moment (t_1) when the magnetic flux has its maximum (the top curve). The spectral data were taken from Fig. 1 of a paper (Kutsenko et al., 2021). The solar magnetogram images obtained by the Helioseismic and Magnetic Imager onboard the Solar Dynamics Observatory spacecraft were used to calculate the spectra.

The dashed curve at the bottom spectrum indicates the best fit by the exponential spectrum Eq. (7) (deterministic chaos) and the dotted arrow indicates the position of k_c .

The dashed curve at the top spectrum indicates the best fit by the stretched exponential Eq. (6) with $\beta = 1/5$ (distributed chaos).

It could be expected that at the onset of the emergence process we will observe deterministic chaos (Bershadskii, 2024c). In contrast, when the magnetic flux has its maximum we will observe a rather strong randomization of the magnetic field. The value $\beta = 1/5$ will be related below to a magneto-inertial range dominated by magnetic helicity in the presence of a mean magnetic field (this value is sufficiently small to consider it as a precursor of hard turbulence).

The randomization can also be described in probabilistic terms, i.e. one can consider probability distributions of the characteristic wavenumber k_c and frequency f_c for deterministic chaos: $P(k_c)$ and $P(f_c)$. In this approach we have for $\beta < 1$:

$$E(k) \propto \int_0^\infty P(k_c) \exp -(k/k_c) dk_c \propto \exp -(k/k_\beta)^\beta \quad (8)$$

$$E(f) \propto \int_0^\infty P(f_c) \exp -(f/f_c) df_c \propto \exp -(f/f_\beta)^\beta \quad (9)$$

The probabilistic approach can be called ‘distributed chaos’.

The Eq. (8) can be used to estimate $P(k_c)$ for large k_c (Johnston, 2006)

$$P(k_c) \propto k_c^{-1+\beta/[2(1-\beta)]} \exp(-\gamma k_c^{\beta/(1-\beta)}) \quad (10)$$

Analogously can be estimated $P(f_c)$ for large values of f_c .

Let us generalize the Eqs. (4) and (5) as

$$B_c \propto k_c^\alpha, \quad B_c \propto f_c^\alpha \quad (11)$$

the parameter α usually take different values for spatial and temporal cases (cf Eqs. (4) and (5)).

A relationship between the exponents β and α can be obtained from the Eqs. (10) and (11) (using some algebra) for the half-normally distributed positive variable B_c (i.e. distribution $P(B_c) \propto \exp -(B_c^2/2\sigma^2)$ and the normal distribution is truncated to only have the nonzero density for positive values of its argument)

$$\beta = \frac{2\alpha}{1+2\alpha} \quad (12)$$

Then it follows from the Eqs. (4), (5), and (12) that

$$E(k) \propto \exp -(k/k_\beta)^{1/5}, \quad E(f) \propto \exp -(f/f_\beta)^{1/4} \quad (13)$$

for the magneto-inertial range dominated by the magnetic helicity in the presence of a considerable mean magnetic field.

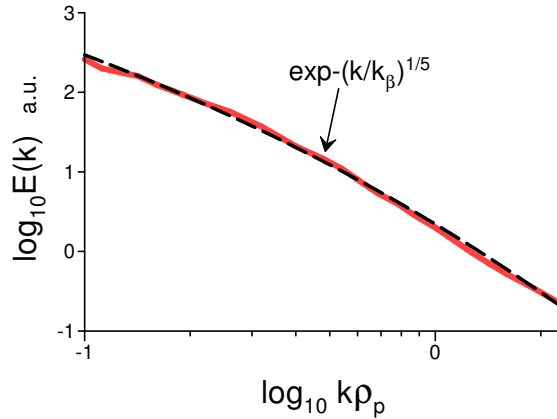


Figure 2: Power spectrum of a magnetic field component in the undisturbed solar wind just before it impacts the Earth’s magnetosphere (the Winds spacecraft mission).

5. Solar wind, magnetosphere, and ionosphere

We have already observed in Fig. 1 an example of the stretched exponential spatial (wavenumber) spectrum Eq. (13) in the active solar photospheric plasma.

Let us now consider another example of the magnetic energy spectrum observed by the Winds spacecraft mission in the solar wind. The Wind spacecraft was put in a Lissajous orbit around the Lagrange point L1 to investigate the undisturbed solar wind just before it impacts the Earth’s magnetosphere.

Figure 2 shows an example of the spatial (wavenumber) magnetic energy spectrum obtained in this investigation (ρ_p is the proton thermal gyroradius). The wavenumber spectrum was obtained from a frequency spectrum (measured by a probe onboard the spacecraft) using Taylor’s ‘frozen-in’ hypothesis with the transformation $k = 2\pi f/V$, where V is the solar wind speed (the frequency spectra, in this case, are mainly representations of the spectra of the spatial structures passing the measuring probe [Monin & Yaglom, 2007](#); [Taylor, 1938](#)). The spectral data were taken from Fig.1b of the paper ([Zhao et al., 2020](#)). The dashed curve indicates the best fit of the spectral data by the stretched exponential Eq. (13).

Next spatial (wavenumber) power spectra of a component of the magnetic field were obtained in the Earth’s magnetosheath - the boundary layer of the magnetosphere resulting from the encounter of the solar wind with the Earth’s bow shock. The observations were produced by the Cluster multispacecraft mission downstream of the quasiparallel bow shock. Figure 3 shows the power spectra obtained using the measurements made by the farthest (bottom curve) and nearest (top curve) from the bow shock Cluster units (d_i is the ion inertial length). The spectral data were taken from Fig. 2 of the paper ([Yordanova et al., 2008](#)). The dashed curves indicate the best fit of the spectra by the stretched exponential Eq. (13).

In a recent paper ([Mestici et al., 2024](#)) results of measurement produced by a vector field magnetometer onboard Swarm A satellite in the ionosphere (inner edge of the magnetosphere) were reported.

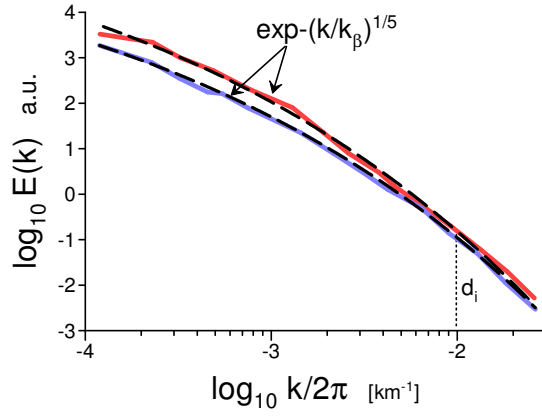


Figure 3: Power spectra of a magnetic field component obtained using the measurements produced by the farthest (bottom curve) and nearest (top curve) from the bow shock Cluster spacecraft units in the Earth’s magnetosheath.

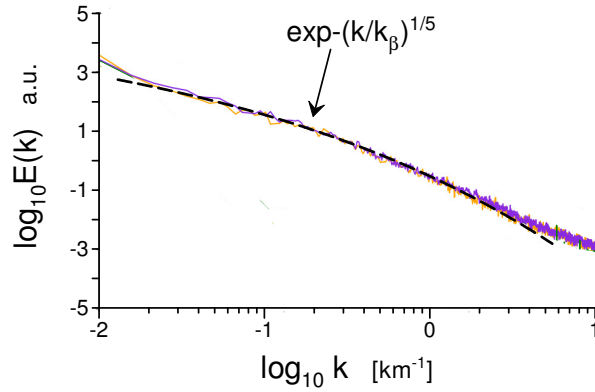


Figure 4: Power spectra of two components of the magnetic field fluctuations perpendicular to the main field observed for quiet geomagnetic conditions in the ionosphere at the Northern polar cap (Swarm satellite mission).

Figure 4 shows the power spectra of two components of the magnetic field fluctuations perpendicular to the main field observed for quiet geomagnetic conditions at the Northern polar cap. The spectral data were taken from Fig. 4 of the paper (Mestici et al., 2024). As in the previous cases (Figs. 2 and 3) the Taylor ‘frozen in’ hypothesis (applicable for the polar cap Mestici et al. 2024) was used to convert the originally measured frequency spectrum into the wavenumber one.

One can see that the two components perpendicular to the main magnetic field have about the same power spectra. The component parallel to the main magnetic field has significantly less energy in comparison to the perpendicular ones.

The dashed curve is drawn to indicate correspondence to the straight exponential Eq. (13).

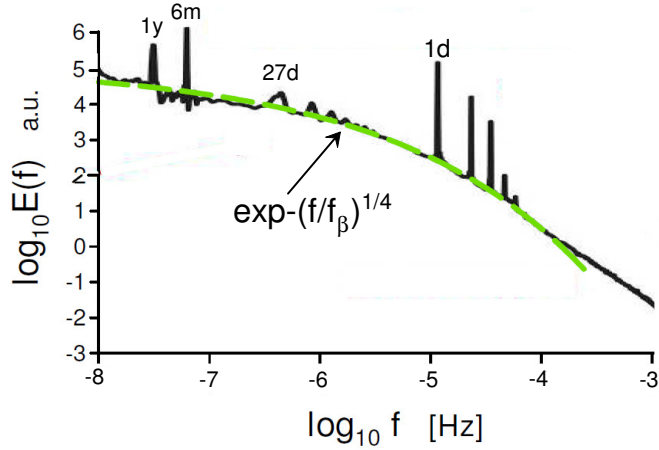


Figure 5: Magnetic energy spectrum at the Earth’s surface obtained using measurements provided by the global magnetic observatory network.

6. Geomagnetic observations at Earth’s surface

6.1. Temporal variability of global magnetic field

Figure 5 shows the magnetic energy spectrum obtained using measurements provided by the global magnetic observatory network at the Earth’s surface. The spectral data were taken from Fig. 1 of the paper (Constable and Constable, 2023). Unlike the frequency spectra obtained in the space plasmas (which are mainly representations of the spectra of the spatial structures passing the measuring probe Monin & Yaglom, 2007; Taylor, 1938) it is a truly temporal spectrum.

The 27-day peak and its harmonics are related to the solar rotation period and reflect the strong solar wind-magnetosphere-ionosphere influence on the *periodic* variability of the magnetic field at the Earth’s surface (see for instance, a recent paper Yu et al., 2021 and Introduction in the present paper about the other prominent peaks in this spectrum related to Sun).

In this paper, we are interested in the chaotic driving of the magnetic field variability at the Earth’s surface by the space and ionospheric plasmas. Therefore the dashed curve in Fig. 5 indicates correspondence to the *frequency* part of the stretched exponential spectral law Eq. (13).

Since both wavenumber and frequency parts of Eq. (13) represent the same physical law Eqs. (4) and (5) (from spatial and temporal points of view respectively) one can conclude that the universal chaotic/turbulent processes in space (solar wind and magnetosphere) and in ionospheric plasmas drive the chaotic temporal variability and determine the level of randomness of the magnetic field at Earth’s surface in the temporal range from a few hours to a few years (see the Section ‘Conclusions and Discussions’ for some practical consequences of the randomness of the magnetic field at the Earth’s surface).

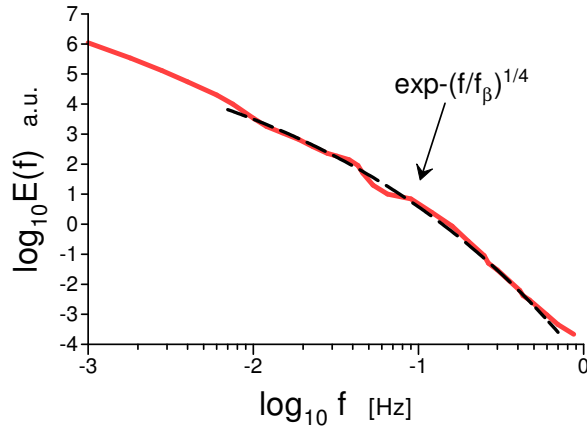


Figure 6: Magnetic energy spectrum at the Earth’s surface during a 200 nT geomagnetic storm time in South Australia.

6.2. A geomagnetic storm over South Australia

Let us consider a specific geomagnetic observation: a 200 nT geomagnetic storm in South Australia. The station’s measurements were made during 12 hours on May 4, 1998 (see for more detail [Constable and Constable, 2023](#); [Fullekrug and Constable, 2000](#)).

The geomagnetic storms are associated with the Sun’s coronal mass ejections. They can substantially increase power in the magnetic energy spectra at Earth’s surface. This is a consequence of a significant increase in the number of solar wind particles, which can put additional pressure on the dayside magnetic field and inject more particles into the Earth’s radiation belts. The dayside magnetic reconnection can open previously closed magnetic field lines and form bundles of opened magnetic field lines (flux ropes). These flux ropes connect the solar wind to the ionosphere ([Akhavan-Tafti et al., 2020](#)), allowing the solar wind plasma to enter into the ionosphere and effectively influence magnetic field fluctuations at the Earth’s surface. Since the idea of the ‘inertial type’ of transfer is based on a non-dissipative transfer of energy and magnetic helicity within the magneto-inertial range (through the ‘eddies’ of different sizes or the waves, see Section 3) one can expect an additional enhancement of the energy and magnetic helicity transfer related to the existence of the magneto-inertial range of scales. This phenomenon is especially significant in the time of the geomagnetic storms.

Figure 6 shows the magnetic energy spectrum for the above-mentioned geomagnetic storm. The spectral data were taken from Fig. 7 of the paper ([Constable and Constable, 2023](#)). The dashed curve in Fig. 6 indicates correspondence to the *frequency* part of the stretched exponential spectral law Eq. (13).

7. Conclusions and Discussion

The temporal behavior of the magnetic field at Earth’s surface apparently reflects the temporal behavior of the magnetic field in the magnetosphere-ionosphere system. Therefore, one can conclude that for this system the temporal magneto-inertial range of scales also ranges from a few hours to a few years.

The possibility of smooth forecasting for magnetic field dynamics at Earth’s surface and for space weather exists due to the stretched exponential spectral behavior typical for

the magneto-inertial range of scales (cf Introduction). Ideally, at smooth forecasting, the predictability horizon can be indefinitely extended by reducing the initial error. In reality, there always exist external limitations related to the smooth forecasting window which in this case is determined by the width of the magneto-inertial range (from a few hours to a few years for the global case).

At non-smooth forecasting (typical for the systems with power-law spectra) the predictability horizon cannot be indefinitely extended by reducing the initial error and the forecasting has inherent inner limitations (Lorenz, 1969). The spatio-temporal patches with power-law (scaling) spectra can appear in the solar wind and magnetosphere-ionosphere's magnetized plasma and request special treatment in this respect. At large scales, their appearance can be related to differences in the fast and slow solar winds and the winds' interaction with the magnetosphere-ionosphere. At small (sub-ion) scales, their appearance can be related to coherent wave activity (e.g. the whistler waves' instability). These phenomena can also be the main factor determining the edges of the smooth forecasting window.

It should be noted that obtaining information about the temporal behavior of the magnetosphere-ionosphere's plasma by the spacecraft-located probes is practically impossible due to Taylor's hypothesis (see, for instance, Bershadskii, 2024b). Therefore this information obtained using the surface stations is rather valuable for understanding and exploring the magnetosphere-ionosphere system. This should be also true for the coupling processes between the solar wind and the magnetosphere-ionosphere system.

References

- Akhavan-Tafti, M. Fontaine, D., Slavin, J. A., Le Contel, O., Turner, D., 2020. Cross-Scale Quantification of Storm-Time Dayside Magnetospheric Magnetic Flux Content. *J. Geophys. Res.: Space Phys.* **125**, e2020JA028027.
- Bershadskii, A., 2024a. Randomization of the Earth's magnetic field driven by magnetic helicity. *Phys. Earth Planet Inter.* **356**, 107250.
- Bershadskii, A., 2024b. Magneto-inertial range dominated by magnetic helicity in space plasmas. *Fundamental Plasma Physics* **11**, 100066.
- Bershadskii, A., 2024c. Small-scale magnetohydrodynamic dynamos: from deterministic chaos to turbulence. E-print [arXiv:2404.0204](https://arxiv.org/abs/2404.0204).
- Borovsky, J.E., 2020. What magnetospheric and ionospheric researchers should know about the solar wind. *J. Atmosph. Solar-Terr. Phys.* **204**, 105271.
- Brandstater, A. and Swinney, H.L., 1987. Strange attractors in weakly turbulent Couette-Taylor flow. *Phys. Rev. A* **35**, 2207-2220.
- Constable, C. and Constable, S., 2023. A grand spectrum of the geomagnetic field. *Phys. Earth Planet Inter.* **344**, 107090.
- Frisch, U. and Morf, R., 1981. Intermittency in nonlinear dynamics and singularities at complex times. *Phys. Rev.* **23**, 2673-2704.
- Fullekrug, M., and Constable, S., 2000. Global triangulation of intense lightning discharges. *Geophys. Res. Lett.* **27**, 333-336.
- Iroshnikov, R.S., 1963. Turbulence of a conducting fluid in a strong magnetic field. *Astronomicheskii Zhurnal* **40**, 742-750 (English translation in *Soviet Astronomy* 1964, **7**, 566-571).

- Johnson, N.L., Kotz, S., and Balakrishnan, N., 1994. Continuous Univariate Distributions, Vol. 1. Wiley NY.
- Johnston, D.C., 2006. Stretched exponential relaxation arising from a continuous sum of exponential decays. *Phys. Rev. B* **74**, 184430.
- Kutsenko, A.S., Abramenko, V.I., and O.K. Kutsenko, 2021. [On the possibility of probing the flare productivity of an active region in the early stage of emergence](#). MNRAS **501**, 6076-6082.
- Khurshid, S., Donzis, D.A., and Sreenivasan, K.R., 2018. Energy spectrum in the dissipation range. *Phys. Rev. Fluids* **3**, 082601(R).
- Kolmogorov A.N., 1941. The local structure of turbulence in incompressible viscous fluid for very large Reynolds numbers. Dokl. Akad. Nauk. SSSR **30**, 301-305.
- Lorenz, E.N., 1969. The predictability of a flow which possesses many scales of motion. *Tellus* **21**, 289–307.
- Maggs, J.E. and Morales, G.J., 2011. Generality of deterministic chaos, exponential spectra, and Lorentzian pulses in magnetically confined plasmas. *Phys. Rev. Lett.* **107**, 185003.
- Maggs, J.E. and Morales, G.J., 2012a. Origin of Lorentzian pulses in deterministic chaos. *Phys. Rev. E* **86**, 015401(R).
- Maggs, J.E. and Morales, G.J., 2012b. Exponential power spectra, deterministic chaos and Lorentzian pulses in plasma edge dynamics. *Plasma Phys. Control. Fusion* **54**, 124041.
- Matthaeus, W.H. and Goldstein, M.L., 1982. Measurement of the rugged invariants of magnetohydrodynamic turbulence in the solar wind. *J. Geophys. Res.* **87**, 6011-6028.
- Mestici, S., Giannattasio, F., DeMichelis, P., Berrilli, F., and Giuseppe, Consolini G., 2024. Scaling properties of magnetic field fluctuations in the high-latitude ionosphere. *Remote Sens.* **16**, 1928.
- Moffatt, H.K. and Tsinober, A., 1992. Helicity in laminar and turbulent flow. *Annu. Rev. Fluid Mech.* **24**, 281-312.
- Monin, A.S., and Yaglom, A.M., 2007. Statistical Fluid Mechanics Vol. II: Mechanics of Turbulence. *Dover Pub. NY*.
- Shebalin, J.V., 2013. Global invariants in ideal magnetohydrodynamic turbulence. *Phys. Plasmas* **20**, 102305.
- Taylor, G.I. 1938. The Spectrum of Turbulence. *Proc. R. Soc. Lond. Ser. A* **164**, 476–490.
- Telloni, D., Carbone, F., Antonucci, E., Bruno, R., et al. 2020. Study of the influence of the solar wind energy on the geomagnetic activity for space weather science. *ApJ* **896**, 149.
- Wu, X.-Z., Kadanoff L.P., Libchaber, A. and Sano, M., 1990. Frequency power spectrum of temperature fluctuations in free convection. *Phys. Rev. Lett.* **64**, 2140-2143.
- Yordanova, E., Vaivads, Andre, Buchert, S.C., and Voros, Z., 2008. Magnetosheath plasma turbulence and its spatiotemporal evolution as observed by the cluster spacecraft. *Phys. Rev. Lett.* **100**, 205003.
- Yu B., Scott C.J., Xue X., Yue X., et al., 2021. A signature of 27 day solar rotation in the concentration of metallic ions within the terrestrial ionosphere. *ApJ* **916**, 106.
- Zhao, G.Q., Lin, Y., Wang, X.Y., Wu, D.J., Feng, H.Q., Liu, Q., Zhao, A., and Li, H.B., 2020. Observational Evidence for Solar Wind Proton Heating by Ion-Scale Turbulence. *Geophysical Research Letters*, **47**, e2020GL089720.